The 8th European Congress on Computational Methods in Applied Sciences and Engineering
ECCOMAS Congress 2022
5-–9 June 2022, Oslo, Norway

A CFD-BASED MULTI-FIDELITY SURROGATE MODEL FOR PREDICTION OF FLOW PARAMETERS IN A VENTILATED ROOM

NINA MOROZOVA[1], FRANCESC XAVIER TRIAS[1], VLADIMIR VANOVSKIY[2], CARLES OLIET[1] AND EVGENY BURNAEV[2]

[1] Heat and Mass Transfer Technological Center, Technical University of Catalonia
Carrer de Colom 11, 08222 Terrassa (Barcelona), Spain; www.cttc.upc.edu
{nina.morozova, francesc.xavier.trias, carles.oliet}@upc.edu

[2] Skolkovo Institute of Science and Technology. Bolshoy Boulevard 30, bld. 1,
121205, Moscow, Russia.

Key words: Multi-fidelity, Surrogate Model, Gaussian Proces Regression, CFD, Indoor Airflow Prediction, Model Predictive Control

Abstract. In this work, we present a multi-fidelity machine learning surrogate model, which predicts comfort-related flow parameters in a ventilated room with a heated floor. The model uses coarse- and fine-grid CFD data obtained using LES turbulence models. The dataset is created by changing the width aspect ratio of the rooms, inlet flow velocity, and temperature of the hot floor. The surrogate model takes the values of temperature and velocity magnitude at four different cavity locations as inputs. These probes are located such that they could be replaced by actual sensor readings in a practical case. The model's output is a set of comfort-related flow parameters. We test two multi-fidelity approaches based on Gaussian process regression (GPR), among them GPR with linear correction (LC GPR), and multi-fidelity GPR (MF GPR) or co-kriging. The computational cost and accuracy of these approaches are compared with GPRs based on single-fidelity data. All of the tested multi-fidelity approaches successfully reduce the computational cost of dataset generation compared to high-fidelity GPR while maintaining the required level of accuracy. The co-kriging approach demonstrates the best trade-off between computational cost and accuracy.

1 INTRODUCTION

Modern heating ventilation and air conditioning (HVAC) systems are required to maintain human thermal comfort and using minumal energy consumption in buildings. Traditionally indoor environments are simulated using reduced-order models and computational fluid dynamics (CFD). Reduced-order models are often unable to achieve sufficient accuracy due to the simplifications adopted. On the other hand, accurate CFD simulations are still prohibitively expensive for most of the practical building applications [1, 2]. Moreover, the situation will not change in the foreseeable future [3]. As a result, new fast and accurate numerical models are needed.

A surrogate model is an engineering method used when an outcome of interest cannot be easily measured or computed, so a model of the outcome is used instead. Surrogate models mimic the behavior of the high-fidelity simulation model as closely as possible while being considerably computationally cheaper to evaluate. Because of its inexpensiveness, surrogate modeling is one of the important trends in the built environment research [4]. Using CFD simulations for surrogate modeling usually results in high computational cost of dataset generation; thus, an increasing number of works is trying to optimize it by using a multi-fidelity approach. It combines a large number of computationally cheap low-fidelity (LF) simulations and a smaller number of expensive high-fidelity (HF) simulations, in way that ensures a trade-off between simulation cost and surrogate model accuracy. For instance, Lamberti & Gorlé [5] combined RANS and LES simulations in order to create a machine learning model which predicts wind loads on buildings. They showed that the proposed multi-fidelity framework has the potential to reduce the number of expensive LES simulations while retaining a higher accuracy than standard reduced-order models. The co-kriging technique was used by Li *et al.* [6] for the optimization of high-speed train cabin ventilation system design, which led to significant savings of computational time. Zhang *et al.* [7] combined HF models using a CFD evaluation with fine grid and the LF models using the same CFD model with a coarse grid to optimize the aerodynamic shape of an airfoil, which outperformed the single-fidelity method. However, to the best of the author's knowledge, multi-fidelity surrogate modeling has not yet been applied to simulations of the indoor environment.

In this work, we propose a CFD-based multi-fidelity surrogate model to predict comfort-related flow parameters in a ventilated room with a heated floor. This particular test configuration includes both natural and forced convection phenomena, making it hard for the classical reduced-order models to achieve meaningful results and making expensive CFD simulations indispensable. However, the surrogate models have the capacity to significantly reduce the simulation cost while maintaining an acceptable level of accuracy. The model's inputs are values of temperature and velocity in the locations, which in a practical case could be replaced by sensor readings. The main novelty of this work is the adoption of a multi-fidelity approach, which allows to substantially decrease the amount of computational resources spent on the dataset generation and increase the prediction capacity by amplifying the set of working conditions.

2 TEST CASE DESCRIPTION

We use the incompressible Navier-Stokes equations for Newtonian fluids with constant physical properties as governing equations of the flow. We adopt the Boussinesq approximation to account for the density variations to model the buoyancy effects. Thermal radiation is neglected. All the results are presented in dimensionless form. The reference values of time, velocity, temperature, and length are $t_{ref} = H/U_{ref}$, $U_{ref} = U_{in}$, ΔT, and H, respectively, where U_{in} is the inlet bulk velocity, H is the cavity heigth, $\Delta T = T_h - T_c$ is the temperature difference.

The physical setup used in this work is a three-dimensional ventilated cavity with a heated floor [8]. This flow configuration presents a mixed convection phenomenon, challenging due to the interaction of both natural and forced convection. It resembles an airflow in a middle section of a room with mixing ventilation and thermal exhausts. The geometry of the studied cavity is shown in Figure 1 (left). Cold air at $T_c = -0.5$ enters the cavity through the long thin inlet at the top of the left wall. The inlet velocity profile in the vertical (y) direction corresponds to a

parabolic Poiseuille flow. The inlet slot has an aspect ratio $A_{in} = h_{in}/H = 0.018/1.04$. The air is discharged through the outlet slot with the aspect ratio $A_{out} = h_{out}/H = 0.024/1.04$ at the bottom of the right wall of the cavity. The bottom wall is maintained at a hot temperature of $T_h = 0.5$, while the three other sidewalls are kept at the cold temperature of T_c.

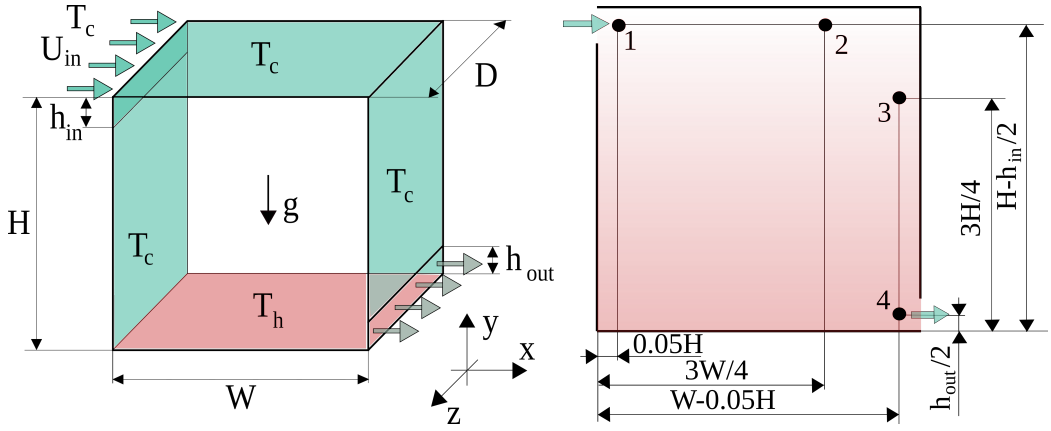

Figure 1: Left: geometry of the studied test case. Right: locations of the input data probes at the mid-depth cavity plane ($z = D/2$).

The cavity is filled with air ($Pr = \nu/\alpha = 0.71$, where ν is the kinematic viscosity and α the thermal diffusivity). The depth aspect ratio of the cavity is $A_d = D/H = 0.3/1.04$, where D is the depth of the cavity. At the outlet, convective boundary conditions ($\partial\phi/\partial t + U_{in}\partial\phi/\partial x = 0$) are imposed for the velocity and temperature. No-slip boundary conditions are applied on the walls. The initial velocity field is set to zero and the initial temperature is set equal to the temperature at the cold wall. Periodic boundary conditions are used in the spanwise (z) direction.

3 DATASET GENERATION

3.1 Description of the dataset

We build the input-output dataset by changing the width aspect ratio of the cavity ($A_w = W/H$), the Rayleigh number based on the cavity height $Ra_H = g\beta\Delta T H^3/(\nu\alpha)$, and the Froude number based on the ratio between the bulk inlet and buoyant velocity ($Fr = U_{in}/U_{buo} = Re_H/\sqrt{Ra_H}$, $Re_H = U_{in}H/\nu$ is the Reynolds number based on the cavity height), where g is the gravitational acceleration and β is the thermal expansion coefficient. Test case configurations used in the generation of the dataset are shown in Table 1.

Chosen combinations of $A_w - Ra - Fr$ are realistic and relevant for indoor environmental applications. For example, assuming that the cavity height is 2.5 meters, the highest Rayleigh number (9.6×10^9) corresponds to a temperature difference of approximately $6°C$. On the other hand, the maximum Reynolds number based on the cavity height used in this work is 9.79×10^5. Considering the same height of 2.5 meters, it corresponds to an inlet velocity of $\approx 1m/s$.

A_w	$\{0.25, 0.50, 1.00, 2.00, 4.00\}$
Ra_H	$\{1.5 \times 10^8, 6.0 \times 10^8, 2.4 \times 10^9, 9.6 \times 10^9\}$
Fr	$\{0.15, 0.20, 0.25, ..., 0.55, 0.60, 0.70, ..., 1.50, 1.60\}$
Total number of low-fidelity (LF) simulations - 360	
Total number of high-fidelity (HF) simulations - 240	
Total number of simulations - 600	

Table 1: Combinations of the test case configurations for generating the CFD dataset.

3.2 Input and output parameters

As input parameters of our surrogate model, we consider cavity width aspect ratio (A_w), temperature (T) and velocity magnitude (V) probes at four different locations on the mid-depth cavity plane ($z = D/2$). In a practical situation, apart from the cavity width aspect ratio, the values of the Froude and Rayleigh numbers are not available; hence, they are discarded from the current study. In total, we use 9 ($A_w + 4T + 4V$) input parameters. The positions of the probes are shown in the figure 1 (right). The positions of the probes are chosen according to the results of our previous work [9]. The probes are located near the walls of the cavity in order to mimic the positions of real temperature and velocity sensors.

As the outputs of the model, we choose two global flow parameters: average Nusselt number on the hot wall - $<Nu>$ and average enstrophy - $<\Omega>$. They represent basic airflow properties and are relevant for thermal comfort [10]. The average Nusselt number is a measure of heat transfer. It is computed using the temperature gradient at the bottom wall surface:

$$<Nu>= -\frac{1}{WD}\int_{x=0}^{W}\int_{z=0}^{D}\frac{\partial <T>}{\partial y}dx\,dz \quad \text{at} \quad y=0, \tag{1}$$

where, the standard bracket "<>" notation is used for time-averaged values. Enstrophy is a measure of turbulence intensity. Enstrophy is directly related to draught and local discomfort. It is averaged over time and cavity volume and calculated as follows:

$$<\Omega>= \frac{1}{WHD}\int_{x=0}^{W}\int_{y=0}^{H}\int_{z=0}^{D} <\boldsymbol{\omega}^2> dx\,dy\,dz, \tag{2}$$

where $\mathbf{u} = (u, v, w)$ is the velocity vector in Cartesian coordinates $\mathbf{x} = (x, y, z)$ and $\boldsymbol{\omega} = \nabla \times \mathbf{u}$ is the vorticity.

4 NUMERICAL METHODS

4.1 CFD simulations

To generate input and output data for the model, we use large-eddy simulations (LES) on staggered grids with second-order symmetry-preserving spatial discretization [11] and a one-parameter fully explicit second-order temporal discretization scheme [12]. To perform the simulations, we use an in-house STG CFD code [13] with the LES-S3PQ turbulence model [14]. The choice of the turbulence model, type of spatial and temporal discretizations, and CFD software

is based on the findings of our previous work [3], where we performed an extensive validation and mesh sensitivity analysis of the same test case ($Ra_H = 2.4 \times 10^9$, $Re_H = 39520$, and $A_w = 1$).

Choosing optimal grid discretization for the CFD simulations is a complex procedure, especially if one plans to perform many simulations simultaneously. On the one hand, the nature of LES turbulence modeling requires sufficient spatial discretization in order to obtain accurate simulation results. Also, the high computational cost of the simulations requires optimizing the grid size by tuning it to the physics and geometry of each test case. As a solution, we have developed an algorithm for the automatic mesh generation based on the variable physical parameters of the experiment (Fr, Ra_H, A_w), previously conducted validations [15, 16], and desired level of mesh refinement. The detailed description of this algorithm could be found in our previous work [9]. For the HF grids, we used grids which are 3 times coarser than direct numerical simulation (DNS) grid in each direction, and for the LF, we used grids 6 times coarser than DNS in each direction.

4.2 Surrogate models

Our work is based on the Gaussian process regression (GPR) approach, which is capable of constructing nonlinear regression models [17] with some guaranteed theoretical properties [18]. A significant advantage of GPR over other machine learning frameworks is the ability to treat variable fidelity data [19], which allows to reduce the computational cost of dataset generation. We investigate the following approaches: GPR for single-fidelity data [20], GPR with linear correction (LC GPR), and multi-fidelity GPR (MF GPR) or co-kriging [21]. All of the models use the open-source machine learning library scikit-learn [22].

GPR [20] is a kernel-based machine learning technique for non-linear regression problems. A Gaussian Process (GP) is a set of random variables, such that any finite subset of these variables have a joint Gaussian distribution. As a distribution, a GP is characterized by its mean and covariance function. In this work we use Matérn covariance function, which is a generalization of commonly used squared exponential covariance function. We test three different single-fidelity GPR: HF-GPR - a model trained only with HF data, LF-GPR - a model trained only with LF data, and HFLF-GPR - a model trained on a mix of LF and HF data without distinguishing the data fidelity.

LC GPR approach is a modification of single-fidelity GPR. The developed surrogate model consists of three steps. In the first step we train a single-fidelity GPR model on LFdata and test it on HF data. In the second step we estimate an error between the test results and the actual HF data and train a linear regression model to predict this error. In the third step we correct the predictions of LF surrogate model for the the step one using the error correction model from the step two. LC GPR approach allows to compensate simulation-induced errors and reduce the amount of HF data used in the model training process.

MF GPR or co-kriging [21] estimates for a poorly sampled variable $\mathbf{y}_l(\mathbf{x})$ with the help of a well-sampled variable $\mathbf{y}_h(\mathbf{x})$. MF GPR attempts to predict the HF process using information (autocorrelation and cross-correlation) in the covariate to make a better prediction:

$$\mathbf{y}_l(\mathbf{x}) = f_l(\mathbf{x}) + \epsilon_l \tag{3}$$

$$\mathbf{y}_h(\mathbf{x}) = c y_l(\mathbf{x}) + y_d(\mathbf{x}), \tag{4}$$

where $y_d(\mathbf{x}) = f_d(\mathbf{x}) + \epsilon_d$ is a new process representing the difference between the HF process and LF process, which will correct the LF data and c is the regression coefficient.

4.3 Data preprocessing and metrics

In our work, we normalize all the input and output data to fit the range of $[-1, 1]$. To improve the prediction results and avoid model overfitting we use cross-validation. In this study, we adopt a leave-one-out (LOO) cross-validation method. This cross-validation procedure maximises the amount of data used for training since only one sample is removed from the training set. All of the HF data not involved in the training process is used for testing. The size of the test dataset varies depending on the analysis performed (see Section 5 for details).

In order to quantify the accuracy of the model, we use mean relative prediction error (MRE), which is designed as follows:

$$MRE(\phi) = \frac{1}{N}\sum_{i=1}^{N}\frac{|\phi_{CFD} - \phi_{SM}|}{|\phi_{CFD}|}, \tag{5}$$

where N is the number of samples in the test dataset, ϕ_{CFD} represents any one of the two comfort-related parameters calculated from the CFD simulations, and ϕ_{SM} represents a prediction from one of the surrogate models. We assume that less than 10% MRE is acceptable for this model.

5 RESULTS

5.1 Single-fidelity models

Here we present a comparison between two single-fidelity models, namely HF-GPR and LF-GPR. Both models are tested on HF data. Nusselt number on the hot wall $<Nu>$ (Figure 2, left) shows steady improvement of accuracy on both HF and LF surrogate models with the increase of the number of samples in the training dataset. Average enstrophy $<\Omega>$ (Figure 2, right) shows very high MREs on a low number of samples for both HF and LF models while significantly improving the results with the increasing number of samples. However, even with the highest available number of samples LF GPR does not reach the accuracy of HF GPR, which is caused by the model-induced errors.

The performance of these two single-fidelity models establishes the baseline for further comparison between the different multi-fidelity approaches. The HF dataset is reduced to 130 data samples since all of the studied flow parameters converge to a steady prediction error at this dataset size. On the other hand, the LF dataset is used entirely since the computational cost of it is lower, and $<\Omega>$ did not reach required accuracy. The extensive comparison between different multi-fidelity approaches is made only for the enstrophy $<\Omega>$ since this flow parameter is the most illustrative example due to the highest LF and HF prediction differences. The results for Nusselt number are summarized in Table 2.

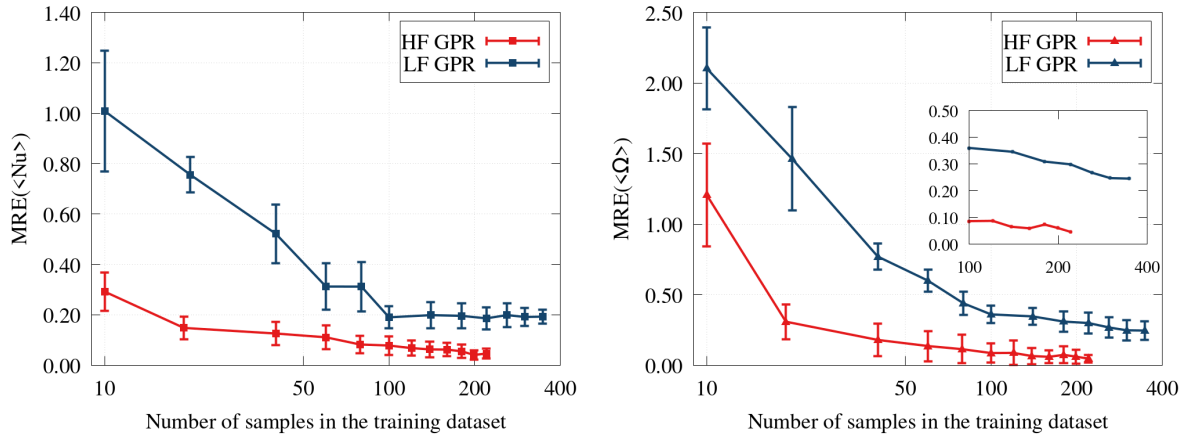

Figure 2: MRE of the studied flow parameters for different number of samples in the training dataset and different single-fidelity models. Left: Nusselt number on the hot wall, $< Nu >$. Right: average enstrophy, $<\Omega>$.

5.2 Multi-fidelity models

The main purpose of using the multi-fidelity approach is to reduce the computational cost without substantial loss of accuracy. The average computational cost of one HF simulation is approximately 2700 core-hours, while the average cost of one LF simulation is 160 core-hours. These numbers are approximated using the whole datasets; however, the computational cost of each individual simulation depends on the physical and geometrical parameters of the test case and is highly variable. Nonetheless, the total computational cost of HF GPR model training is 351 kilo-core-hours (Kh), which is considered the maximum reference computational cost.

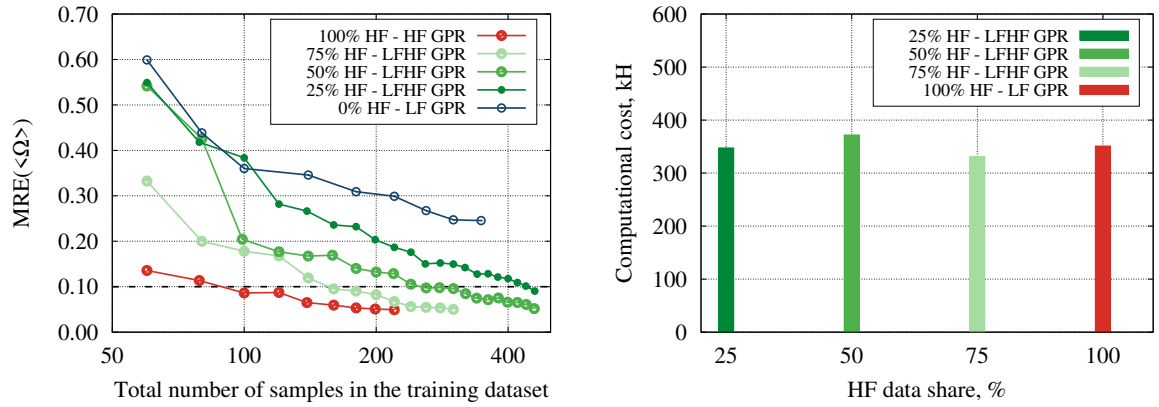

Figure 3: HFLF GPR model. Left: MRE of the average enstrophy $<\Omega>$ for a different total number of training samples and different percentage of HF samples. Right: Computational cost of dataset generation for accurate predictions (< 0.1) using different percentages of HF samples.

Figure 3 (left) shows the MRE of the average enstrophy $<\Omega>$ predicted using the HFLF GPR model. The horizontal axis is the total number of samples in the training dataset, and

the vertical axis is $MRE(<\Omega>)$. Each plot line is obtained by changing the percentage of HF samples in the training dataset. The blue line (0% HF) is the single-fidelity model, trained only on LF data, while the red line (100% HF) is the HF model. The dotted black line marks the $MRE(<\Omega>) = 0.1$ - the required accuracy. Even the small number of HF samples introduced in the dataset successfully improves the model's accuracy to an acceptable level. Figure 3 (right) shows the computational cost, $[Kh]$ of CFD simulations, which were required to achieve the desired accuracy ($MRE < 0,1$) for each of the studied dataset configurations. Only the HFLF GPR model with 75% of HF samples could reduce the computational cost by 6% compared to the baseline HF model. The reason is that there is no distinction between the samples' fidelity; thus, the model's accuracy mostly depends on the amount of HF data samples.

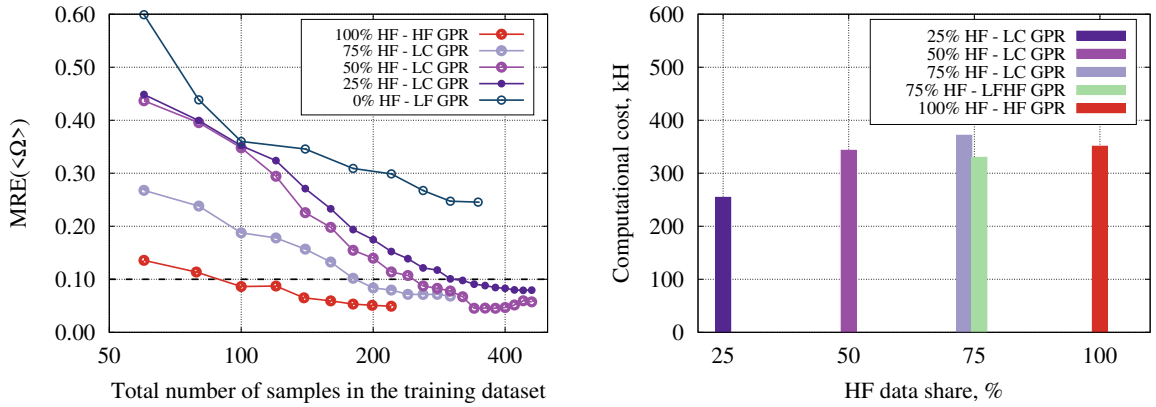

Figure 4: The same caption as Figure 3, but for LC GPR model.

The accuracy of the LC GPR model is shown in Figure 4 (left). LC GPR model has relatively low accuracy for the small number of samples, but when more than 200 samples are used, it is improved substantially. Moreover, the percentage of HF samples in the correction step does not significantly influence the accuracy, which allows to reduce the computational cost. Figure 4 (right) shows the computational cost of different configurations of LC GPR models in comparison with single-fidelity models. LC GPR model has substantial advantages over both HF GPR and HFLF GPR, resulting in 28% lower computational cost since it has achieved the required prediction error using only 25% of HF samples.

Figure 5 (left) shows the MRE of the average enstrophy by MF GPR model for different configurations of the training dataset. The model is performing similarly to the HFLF GPR and LC GPR; however, it needs smaller datasets in order to reach the desired prediction accuracy. This makes the model computationally cheaper than the others (Figure 5, right) since it requires 25 HF samples with a total of less than 300 samples to reach an MRE lower than 0.01 (32% reduction in computational cost). This makes the MF GPR model the most efficient among the studied multi-fidelity models.

The computational cost mostly depends on the amount of HF data; thus, it is interesting to see more closely how it influences the accuracy. In Figure 6 (left), we plot the $MRE(<\Omega>)$ for the studied models using a different number of HF samples. The number of LF samples is constant and is equal to 350. The big blue point on the left corresponds to the $MRE(<\Omega>)$,

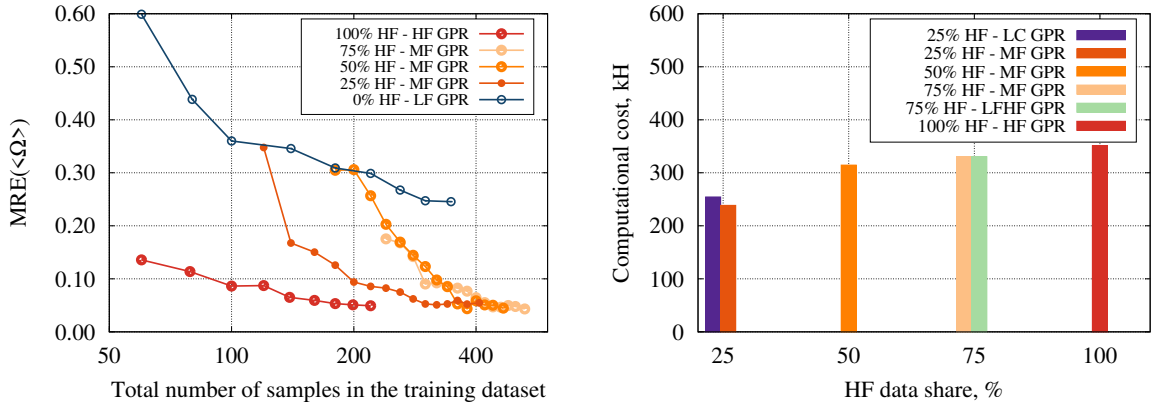

Figure 5: The same caption as Figure 3, but for MF GPR model.

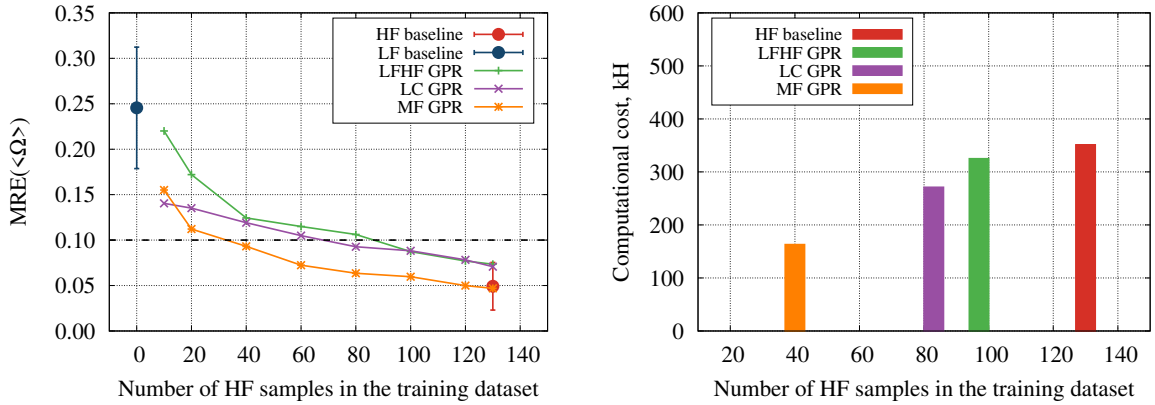

Figure 6: Left: MRE of the average enstrophy $<\Omega>$ for different number of HF training samples using different surrogate models. Right: Computational cost of dataset generation for accurate predictions (< 0.1) using different number HF samples with different surrogate models.

obtained using the LF GPR model, while the red point on the right corresponds to the HF GPR model, respectively. All of the approaches show a similar tendency and steadily improve the prediction with the increase in the HF data. However, the MF GPR model requires the least amount of HF samples to reach the required prediction accuracy, while the HFLF model needs considerably more samples. Figure 6 (right) shows the minimal computational cost at which the required accuracy was reached for the tests on the left. Both MF GPR and LC GPR models successfully reduce the computational cost by 55% and 23% respectively), since they are aware of the fidelity of each sample and learn from the existing dataset more efficiently. On the other hand, the HFLF GPR model results in is very close to the HF GPR model (7% reduction) since it simply mixes the data, which results in a higher computational cost.

Table 2 summarises the configurations of training datasets which showed the best trade-off between computational cost and accuracy for each of the studied surrogate modeling approaches. These configurations are based on the analysis of Figures 3-6, where the mean relative prediction

Model	Samples			MRE		Comp cost,	Reduction,
	HF	LF	total	$<Nu>$	$<\Omega>$	[Kh]	[%]
HF GPR	130	-	130	0.046 ± 0.02	0.046 ± 0.03	351	-
LF GPR	-	350	350	0.193 ± 0.03	0.246 ± 0.07	100	-
HFLF GPR	100	350	450	0.042 ± 0.06	0.093 ± 0.05	335	7%
LC GPR	75	225	240	0.112 ± 0.06	0.100 ± 0.05	254	28%
MF GPR	40	350	380	0.092 ± 0.04	0.093 ± 0.05	164	55%

Table 2: MRE of the studied flow parameters, computational cost and number of low- and high-fidelity dataset samples of the studied models with the best trade-off between computational cost and accuracy.

error of the enstrophy was plotted. The multi-fidelity models have higher accuracy than the single-fidelity model trained only on HF data and reduced the computational cost compared to the baseline HF model. The prediction errors are very similar for all of the multi-fidelity models. However, the MF GPR has the lowest dataset generation cost.

6 DISCUSSION AND CONCLUSIONS

In this work, we presented a multi-fidelity machine learning surrogate model, combining a large number of computationally efficient coarse grid LES simulations with a smaller number of fine grid HF LES. The model predicts the comfort-related flow parameters in a three-dimensional ventilated cavity with a heated floor. The developed surrogate model provides almost instant accurate predictions using an ordinary office computer and requires less training computational resources than a similar single-fidelity model. The model's input parameters are the temperature and velocity magnitude values at different probe locations within the cavity domain. The output parameters are the average Nusselt number and the average enstrophy. The input data of the developed model is structured to take the values of temperature and velocity in the locations, which could be replaced by sensor readings. The main computational burden of the surrogate model is the cost of its development because, at this step, a comprehensive set of HF data is required. The training data was generated using the MareNostrum 4 supercomputer at the Barcelona Supercomputing Center. We limited ourselves to 750Kh core-hours computational resources; we spent 650Kh on 240 HF CFD simulations and 100Kh on 350 LF simulations. In order to create the dataset, we were changing three physical parameters of the cases - Froude number, Rayleigh number, and the cavity width aspect ratio. The range in which these parameters were varying was chosen to represent the realistic indoor environments.

Three different multi-fidelity approaches, namely HFLF GPR, LC GPR, and MF GPR, were compared against two single-fidelity models - HF GPR and LF GPR. All of the models are based on Gaussian process regression with Matérn kernel function. All models were validated on HF data, and the validation results were averaged over 15 runs. The use of multi-fidelity models reduced the computational cost considerably. Even a simple HFLF GPR model is less computationally expensive than the baseline HF GPR model. More sophisticated multi-fidelity models like LC GPR and MF GRP required 55% less computational resources than the HF GPR model. LC GPR does not perform as well as the MF GPR since it is a simpler linear model. It

corrects the estimated error between HF and LF data, which does not always improve the resulting accuracy because the errors are not necessarily proportional to the model input parameters. The MF GRP has shown the best trade-off between computational cost and accuracy among studied multi-fidelity models. It has the potential to significantly reduce the number of costly CFD simulations needed for training while providing notably higher accuracy than standard reduced-order models. Nonetheless, a broad study is required on a proper choice of HF data to further reduce the computational cost and increase the range of operation conditions.

Acknowledgments

This work has been financially supported by the project RETOtwin [PDC2021-120970-I00] funded by MCIN/AEI/10.13039/501100011033 and European Union Next Generation EU/PRTR. N. Morozova is supported by the by the Ministerio de Economía y Competitividad, Spain [FPU16/06333 predoctoral contract]. E. Burnaev is supported by RFBR grant 21-51-12005 NNIO_a. C. Oliet, is suppoted by the Catalan Government as a Serra Húnter lecturer. The calculations were performed on the MareNostrum 4 supercomputer at the Barcelona Supercomputing Center [RES project IM-2021-1-0015]. The authors thankfully acknowledge these institutions.

REFERENCES

[1] N. Morozova, R. Capdevila, F. X. Trias, and A. Oliva. Towards real-time CFD simulation of indoor environment. In *Proceedings of 10th International Conference on Computational Fluid Dynamics, ICCFD10*, July 9-13, 2018.

[2] N. Morozova, R. Capdevila, F. X. Trias, and A. Oliva. On the feasibility of CFD for transient airflow simulations in buildings. In *Proceedings of Building Simulation 2019: 16th Conference of IBPSA, BS19*, September 2-4, 2019.

[3] N. Morozova, F. X. Trias, R. Capdevila, C. D. Pérez-Segarra, and A. Oliva. On the feasibility of affordable high-fidelity CFD simulations for indoor environment design and control. *Build Environ*, 184:107144, 2020.

[4] P. Westermann and R. Evins. Surrogate modelling for sustainable building design – A review. *Energy Build*, 198:170–186, 2019.

[5] C. Lamberti, G.and Gorlé. A multi-fidelity machine learning framework to predict wind loads on buildings. *J Wind Eng Ind Aerodyn*, 214:104647, 2021.

[6] N. Li, L. Yang, X. Li, X. Li, J. Tu, and S. C. P. Cheung. Multi-objective optimization for designing of high-speed train cabin ventilation system using particle swarm optimization and multi-fidelity Kriging. *Build Environ*, 155:161–174, 2019.

[7] X. Zhang, T. Xie, F.and Ji, Z. Zhu, and Y. Zheng. Multi-fidelity deep neural network surrogate model for aerodynamic shape optimization. *Comput Methods in Appl Mech Eng*, 373:113485, 2021.

[8] D. Blay, S. Mergui, J. L. Tuhault, and F. Penot. Experimental turbulent mixed convection created by confined buoyant wall jets. In *Proceedings of the 1st EUROTHERM Conference*, pages 821–828, 1992.

[9] N. Morozova, F. X. Trias, R. Capdevila, E. Schillaci, and A. Oliva. A CFD-based surrogate model for predicting flow parameters in a ventilated room using sensor readings. *Energy Build*, 266:112146, 2022.

[10] Ergonomics of the thermal environment — Analytical determination and interpretation of thermal comfort using calculation of the PMV and PPD indices and local thermal comfort criteria. Standard, ISO, 2005.

[11] R. W. C. P. Verstappen and A. E. P. Veldman. Symmetry-preserving discretization of turbulent flow. *J Comput Phys*, 187(1):343–368, 2003.

[12] F. X. Trias and O. Lehmkuhl. A self-adaptive strategy for the time integration of Navier-Stokes equations. *Numer Heat Transf B: Fundam*, 60(2):116–134, 2011.

[13] A. Gorobets, F. X. Trias, M. Soria, and A. Oliva. A scalable parallel Poisson solver for three-dimensional problems with one periodic direction. *Comput Fluids*, 39(3):525–538, 2010.

[14] F. X. Trias, D. Folch, A. Gorobets, and A. Oliva. Building proper invariants for eddy-viscosity subgrid-scale models. *Phys Fluids*, 27(6), 2015.

[15] N. Morozova, F. X. Trias, R. Capdevila, and A. Oliva. Investigating the capabilities of CFD-based data-driven models for indoor environmental design and control. In *Proceedings of 14th WCCM & ECCOMAS Congress 2020,*, 2021.

[16] N. Morozova, F. X. Trias, R. Capdevila, and A. Oliva. Data-driven prediction of flow parameters in a ventilated cavity. In *Proceedings of Building Simulation 2021: 17th Conference of IBPSA, BS21*, September 1-3, 2021.

[17] M. Belyaev, E. Burnaev, E. Kapushev, M. Panov, P. Prikhodko, D. Vetrov, and D. Yarotsky. GTApprox: Surrogate modeling for industrial design. *Adv Eng Softw*, 102:29–39, 2016.

[18] A. Zaytsev and E. Burnaev. Large scale variable fidelity surrogate modeling. *Ann Math Artif Intell*, 81(1-2):167–186, 2017.

[19] N. Klyuchnikov and E. Burnaev. Gaussian process classification for variable fidelity data. *Neurocomputing*, 397:345–355, 2020.

[20] C. E. Rasmussen. *Gaussian Processes in Machine Learning*, pages 63–71. Springer Berlin Heidelberg, 2004.

[21] M. C. Kennedy and A. O'Hagan. Predicting the output from a complex computer code when fast approximations are available. *Biometrika*, 87(1):1–13, 2000.

[22] F. Pedregosa, G. Varoquaux, A. Gramfort, V. Michel, B. Thirion, O. Grisel, M. Blondel, P. Prettenhofer, R. Weiss, V. Dubourg, J. Vanderplas, A. Passos, D. Cournapeau, M. Brucher, M. Perrot, and E. Duchesnay. Scikit-learn: Machine learning in Python. *J Mach Learn Res*, 12:2825–2830, 2011.